Pergamon

Acta mater. Vol. 46, No. 4, pp. 1297–1305, 1998

Printed in Great Britain
PII: S1359-6454(97)00299-1
1359-6454/98 $19.00 + 0.00

INFRARED JOINING OF TiAl INTERMETALLICS USING Ti–15Cu–15Ni FOIL—II. THE MICROSTRUCTURAL EVOLUTION AT HIGH TEMPERATURE

S. J. LEE[1], S. K. WU[1] and R. Y. LIN[2]

[1]Institute of Materials Science and Engineering, National Taiwan University, Taipei, Taiwan 106, Republic of China and [2]Department of Materials Science and Engineering, University of Cincinnati, Cincinnati, OH 45221, U.S.A.

(Received 4 April 1997; accepted 25 July 1997)

Abstract—The microstructural evolution of TiAl joint during infrared joining at 1150°C under different holding times using Ti–15Cu–15Ni foil as brazing filler metal was investigated. Based on the observed microstructures, a five-step microstructural evolution mechanism at 1150°C joining temperature is proposed in this study. These time-dependent evolution steps including (a) β-Ti layer formation, (b) columnar $\alpha + \beta$ two-phase zone formation, (c) α_2-phase nucleation, (d) high Al% α-phase formation and (e) α_2-phase integration, are consistent with the multiphase diffusion theories in solid-state systems. Since different joining temperatures (T_w) have different corresponding ternary isotherms and stable phases, small variations of T_w can result in significant changes of the microstructural morphologies, especially concerning the microstructural evolution of zones of α_2- and the high Al% α-phases. The mechanism proposed in this study has predicted such evolutions, which agree well with observed microstructures. All the observed microstructures at ambient temperatures can be clearly elucidated by this proposed mechanism. © *1998 Acta Metallurgica Inc.*

1. INTRODUCTION

With their many outstanding properties, titanium-aluminides have a high potential to become one of the important high-temperature structural materials. However, appropriate joining techniques are indispensable for the full utilization of these materials due to their low ductility and poor formability at ambient temperatures. Several joining techniques, including welding [1–3], diffusion-bonding [4–6] and infrared joining [7, 8] have been applied in order to develop a suitable process for joining titanium-aluminides. Infrared joining was adopted in this study mainly due to its sensitive thermal response and its rapid, simple and economical advantages [7].

In Part I of this study [9], we used the Ti–Al–Ni(Cu) pseudo-ternary diffusion-path diagrams to discuss the observed multilayered structures including the high-temperature phase(s) of each layer and the phase-transformation of each phase during rapid cooling. Based on the results of Part I, the multilayered interfacial microstructure was mainly formed by the atomic interdiffusion at high joining temperature T_w, which included the primary isothermal solidification of new solid layers and the following solid-state interdiffusion between these layers and the base metal. Due to the solid-state interdiffusion, the multilayered interfacial structure had formed at T_w, and then it phase-transformed to the room-temperature microstructures during rapid cooling. The successively inward diffusion of Al atoms was found to be the main controlling factor. As to the microstructural evolution, however, why or how these multilayered structures evolved at T_w has still not been clarified. In Part II of this study, we focus our investigation on the time-dependent microstructural evolution at 1150°C and the different T_w effects on this evolution. Because of the sensitive response of infrared joining, the microstructural evolution of the joint interface can be effectively realized.

2. EXPERIMENTAL PROCEDURES

In order to investigate the time-dependent microstructural evolution, four infrared joining conditions were carried out at $T_w = 1150$°C with different holding time, t_w. They are (1)##1: $t_w = 18$ s, (2)##2: $t_w = 30$ s, (3)##3: $t_w = 42$ s and (4)##4: $t_w = 60$ s. Here, T_w and t_w are infrared joining temperature and time, respectively, as shown in Fig. 1 of Part I of this study [9]. Material preparation procedures, the joining configurations and the treatments afterwards are in the same manner as described in the Part I of this study [9]. The real holding times for samples ##1 ~ ##4 were 4, 16, 28 and 46 s, respectively.

The microstructural evolution analyses are based on the acquired room-temperature interfacial structural of samples ##1 ~ ##4. As mentioned in Section 4.2 of Part I [9], the acquired 1150°C diffusion-path profiles do not come across any Ni(Cu)-

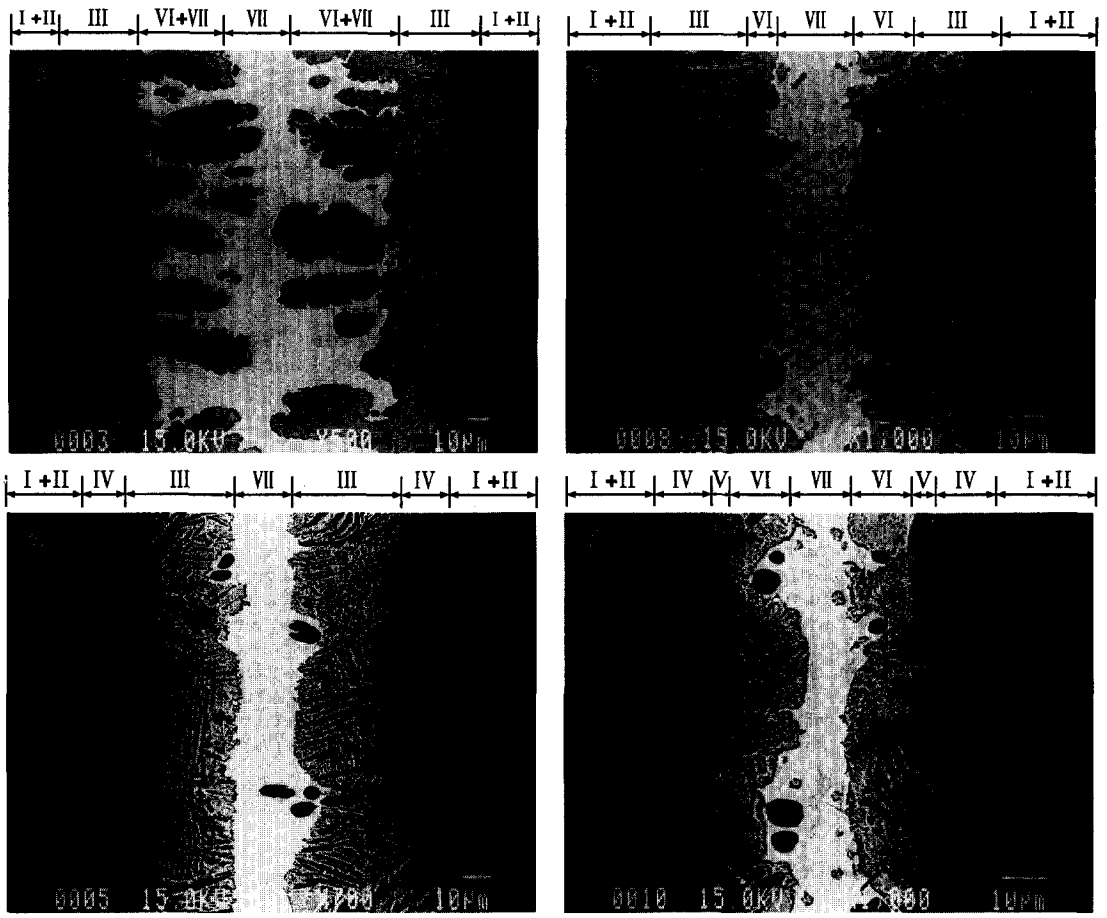

Fig. 1. The back-scattering electron images (BEIs) of four joint interfaces which are joined at $T_w = 1150°C$ with (a) $t_w = 18$ s, (b) $t_w = 30$ s, (c) $t_w = 42$ s and (d) $t_w = 60$ s.

base solid phase on the 1150°C Ti–Al–Ni(Cu) ternary isotherm. All the white precipitates in the joint interfaces are merely formed by the cooling phase transformation. The zone having a similar morphology in the joint interface is regarded as a single-phase region at T_w (the characteristic zones shown in Part I of this study [9]), thus the high-temperature phases in the joined interface can be approximately estimated. Therefore, joint interfacial microstructures varying with different t_w's can be generalized. At the same time, a high-temperature microstructural evolution mechanism with several time-dependent steps can be proposed and discussed by the multiphase diffusion theories in solid-state interdiffusion systems [10–12]. The analyses of joining temperature effects are based on this evolution mechanism. By adding the possible thermodynamic effects of T_w on this mechanism, the time-dependent microstructural evolution at different T_w can also be clearly elucidated. The experimental results of this paper will also be compared with the observed microstructures of samples joined at 1100°C × 30 s and 1200°C × 30 s.

3. EXPERIMENTAL RESULTS

Figure 1(a) ∽ (d) show the back-scattering images (BEIs) of joint interfaces for specimens ##1 ∽ ##4 joined at $T_w = 1150°C$ with $t_w = 18$ s, 30 s, 42 s and 60 s, respectively. Figure 2(a) ∽ (d) are the secondary electron images (SEIs) with Ti, Al, Cu and Ni line scanning profiles (LSPs) for samples ##1 ∽ ##4 of Fig. 1, respectively. All joint interfaces show typical multilayered structures and Cu and Ni atoms are mainly concentrated in the central region.

In Figs 1 and 2, I ∽ VII express the seven characteristic interfacial zones, as mentioned in Section 3.2 of Part I of this study [9]. Before cooling, their corresponding high-temperature phases are γ-TiAl (Zones I & II), $\alpha + \beta$ mixed two-phase (Zone III), high Al% α-phase (Zone IV), α_2-Ti_3Al (Zone V), β-Ti (Zone VI) and the residual liquid filler metal (Zone VII), respectively. These relationships between the high-temperature phases and the observed zones are the basis of our discussions in Section 4.1 of this paper.

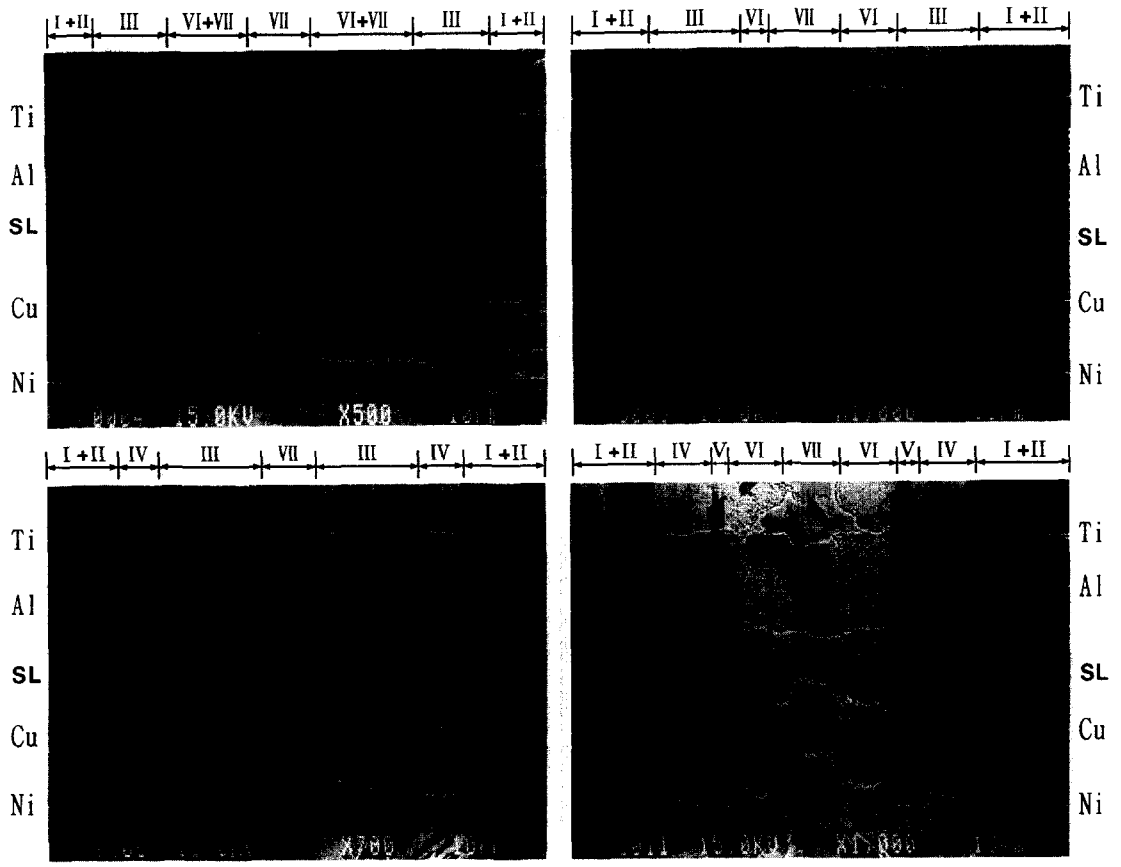

Fig. 2. The secondary electron images (SEIs) with Ti, Al, Cu and Ni LSPs, from top to bottom, of four joint interfaces which are joined at $T_w = 1150°C$ with (a) $t_w = 18$ s, (b) $t_w = 30$ s, (c) $t_w = 42$ s and (d) $t_w = 60$ s.

Figure 2 clearly shows several abrupt drops on the LSP curves of Cu and Ni atoms, as indicated by arrows in Figs 2(b), (c) and (d), when the scanning line (SL) crosses the regions of black α-base phases. According to the multiphase diffusion theories [10–12] in a diffusion couple system, all elements must simultaneously diffuse upon their own activity gradient which is the real driving force behind the interdiffusion of each element. In order to keep the necessary driving force for further interdiffusion, all the activity (a) profiles for elements must continuously vary from one side to another side. Therefore, these abrupt drops of composition (C) imply that Ni(Cu) atoms have a higher activity coefficient(γ) in the black α-base phase than in the β-Ti region due to the fact that $a = C \times \gamma$. The different activity nature of specific atoms in different phases also has a great influence on the microstructural evolution, as will be discussed in Section 4.1.2.

4. DISCUSSIONS

4.1. The microstructural evolution of the infrared joint interface at $T_w = 1150°C$

Based on the observed microstructures of Figs 1 and 2, a five-step mechanism of the microstructural evolution of the infrared joint interface at 1150°C is proposed, as schematically plotted in Fig. 3(a) ∽ (e). According to the observed microstructures and the processing time variation, this five-step mechanism includes (a) β-Ti layer formation, (b) columnar $\alpha + \beta$ two-phase zone formation, (c) α_2-phase nucleation, (d) high Al% α-phase forming and (e) α_2-phase integration. Before further discussion of these steps of microstructural evolution, it is worthy to note that, due to the local equilibrium requirement, all the evolved phases must be the stable ones at T_w, as seen from the 1150°C Ti–Al–Ni(Cu) pseudo-ternary diffusion-path isotherm of Fig. 4 and the Ti–Al binary diagram of Fig. 5.

Figure 4 is a 1150°C Ti–Al–Ni(Cu) pseudo-ternary isotherm in which the compositional loci of joint interfaces of samples ##2 and ##4 are both plotted. The phases indicated on the Ti–Al and Ti–Ni(Cu) abscissas correspond to the phases on the reported 1150°C isotherm in the Ti–Al [13, 14] and in the Ti–Ni [15] binary phase diagram, respectively. The proposed compositional regions of the evolved stable phases are also indicated in Fig. 4, which are based on the reported Ti–Al–Ni ternary 1150°C isotherm [16] and are a modified isotherm according to the acquired diffusion path diagrams

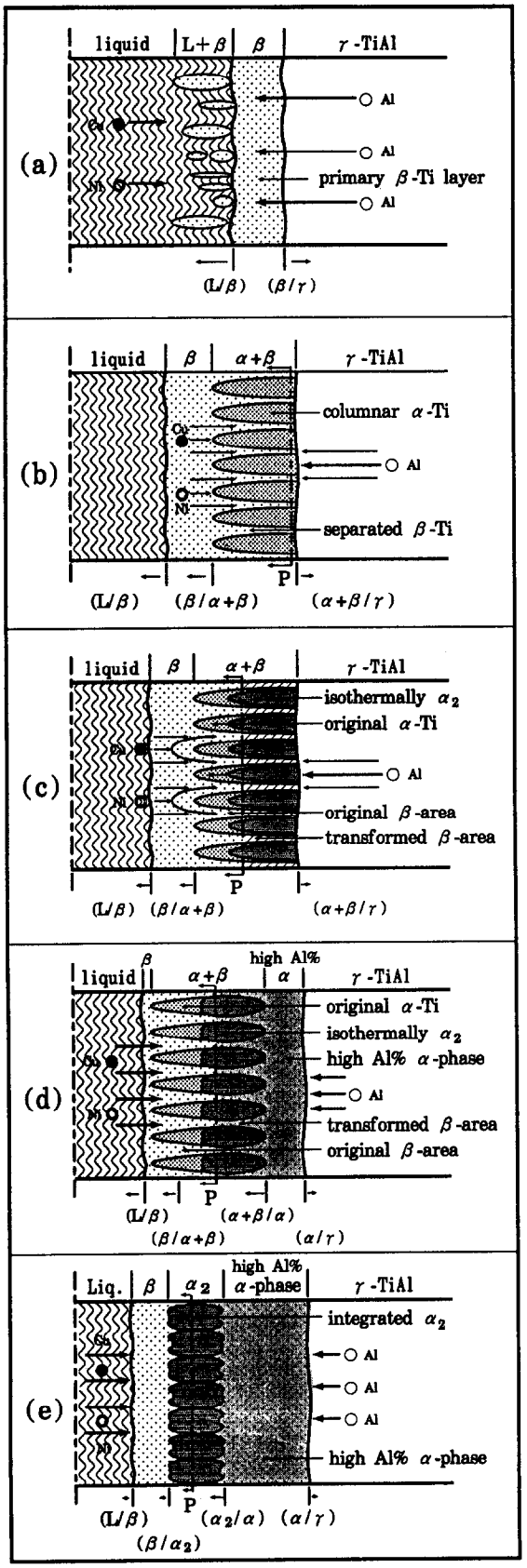

Fig. 3. The schematic profiles showing the proposed five-step microstructural evolution mechanism of infrared joint interface at $T_w = 1150°C$. (a) ∽ (e) are the five time-dependent evolution steps discussed in the text.

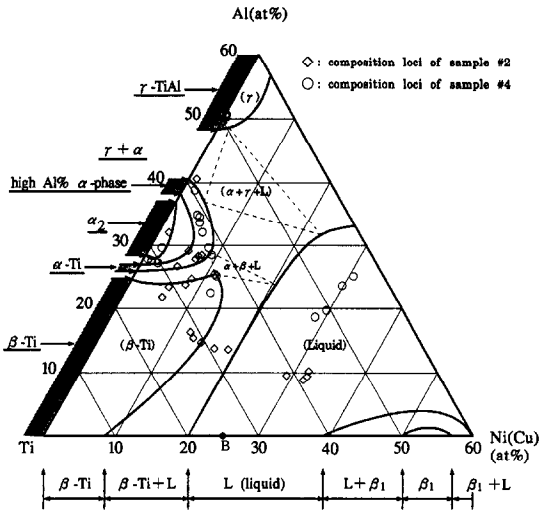

Fig. 4. The 1150°C Ti–Al–Ni(Cu) pseudo-ternary diffusion-path isotherm in which the compositional loci of joint interfaces of samples ##2 and ##4 are both plotted. A and B indicate the composition loci of the original base metal and filler metal, respectively.

whose analytic results are shown in Part I of this study [9]. Except for the area near the β/L interface, all compositional loci in Fig. 4 are concentrated and continuously vary in their own single-phase regions. This feature is consistent with the rules of solid-state multiphase diffusion theories [10–12] and implies that their corresponding zones are formed by the solid-state interdiffusion. It was observed that Zone VI (β-Ti) of sample ##2 near the β/L interface has some compositional loci located outside its 1150°C single-phase region. Because the atomic diffusivity in the liquid is rather fast, the cooling solidification effects may occur and affect

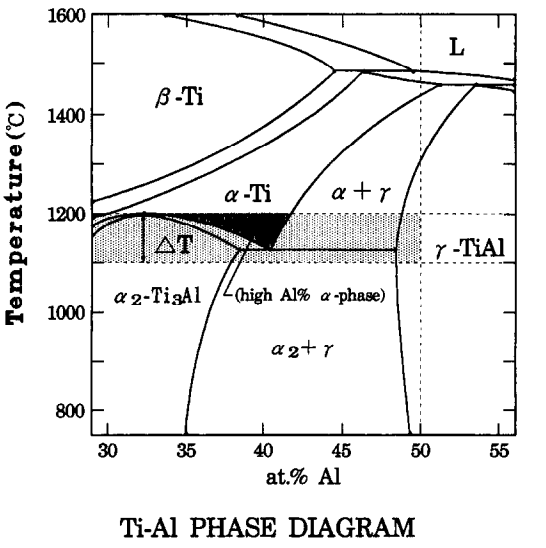

Ti-Al PHASE DIAGRAM

Fig. 5. The central portion of Ti–Al binary phase diagram [13, 14]. The gray shadow area indicates the interested region involved in this study. The black shadow area and ΔT are the high Al% α-phase and the supercooling of α_2-phase at a specific T_w, as defined in the text.

the compositions of this β/L interface during fast cooling, even if the estimated cooling rate is as high as about 1000°C/min.

Figure 5 is the central portion of Ti–Al binary phase diagram [13, 14], in which the gray shadow area is the region involved in this study. The black shadow area shows the high Al% α-phase domain and ΔT represents the supercooling of α_2 phase at a specific T_w. They will be further discussed in the following sections.

4.1.1. Step (1): The β-Ti layer formation. At the beginning of infrared joining at 1150°C, due to the successively inward diffusion of Al atom from the TiAl base metal, one new solid layer (primary layer) will be formed on the liquid/solid (L/S) interface by the isothermal solidification, as shown in Fig. 3(a). From the diffusion-path diagrams as shown in Fig. 4, this primary layer should be the β-Ti phase. This isothermally solidified β-Ti phase is the base of the following solid-state interdiffusion. When the β-Ti layer has formed on the L/S interface and grown into the liquid filler metal, there is a solid/solid (β/γ) interface near the base-metal. Therefore, the solid-state interdiffusion occurs and then the secondary solid phase (α-Ti) and other new phases will be successively formed from this β/γ interface.

At the onset of isothermal solidification, the L/S interface is unstable due to the rapid atomic interdiffusion rates and the dissolution effects of base metal. Therefore, for a short t_w, the joint interface shows a wide $L + \beta$ two-phase zone having a columnar L/β, as shown in Figs 1(a) and 3(a). While for longer t_w, the L/β interface will successively move inward and gradually become a planar one which is a more stable interface based on the surface energy lowering principle, as shown in Fig. 1(c) and (d).

4.1.2. Step (2): The columnar α + β two-phase zone formation. As more Al diffuses in, the α-Ti phase starts to isothermally nucleate and grow on the β/γ interface, as predicted in Fig. 4. Initially, a columnar $\alpha + \beta$ two-phase zone will be formed, as shown in Fig. 3(b). This phenomena is produced by the isothermal β-Ti $\rightarrow$ α-Ti interfacial reaction. As shown in Fig. 3(b), in $\alpha + \beta$ two-phase zone, the black columns indicate the Al-rich α-Ti phase and the areas between them are the Ni(Cu)-rich β-Ti regions. Because the Al atom is a α-Ti stabilizer but Cu and Ni atoms are β-Ti ones [17], the resultant interfacial morphology should have a typical two-phase mixed structure composed of α-stabilized α-Ti and β-stabilized β-Ti regions. This type of elemental partition phenomenon is usually found in some commercial Ti-alloys, such as the Ti-6242 alloy [18], especially when its microstructure is formed by a slower cooling rate during the β-Ti $\rightarrow$ α-Ti cooling phase-transformation [17].

The $\alpha + \beta$ two-phase morphology is allowed in a ternary or quaternary interdiffusion system due to this system having an extra degree of freedom [11, 12]. According to the diffusion-path theorems proposed by Kirkaday [12] and adopted by Van Loo [11], a columnar two-phase zone is produced when a diffusion path passes through a two-phase region from a single-phase one at an angle to the tie lines but then exits into another phase. Thus, at the onset of the isothermal β-Ti $\rightarrow$ α-Ti interfacial reaction, it is believed that the interfacial diffusion-path, which is determined by the nature of elements, will take an angle to the tie lines when it passes through the $\alpha + \beta$ two-phase region. Therefore, from the viewpoint of local equilibrium, the compositional loci of α-Ti and β-Ti phase will vary along their individual two-phase boundary, respectively, as shown in the diffusion-path diagram of sample ##2 in Fig. 4. By this way, a columnar $\alpha + \beta$ two-phase zone will be formed at the joint interface.

As mentioned in Section 3, because Ni(Cu) atoms have a higher activity coefficient in the α-phase than in the β-phase, Ni(Cu) atoms will be expelled from the growing α-Ti regions. This feature will make Ni(Cu) atoms outwardly diffuse mainly along the β-phase areas and let the α-Ti prefer to grow on the tips of the already formed α-Ti columns. At the same time, Ni(Cu) atoms will be concentrated on the β-Ti areas. Then, the elemental partition phenomena occurs and a typical $\alpha + \beta$ two-phase mixed zone is formed, as shown in Fig. 3(b). This $\alpha + \beta$ two-phase zone will continue to grow until it completely fills the primary β-layer or until it meets some effective diffusion barriers, such as the α_2-layer forming at the joint interface.

The above analyses are based on the ideal case in which no lateral diffusion occurs and all α-Ti columns are equal in size on the cross-sectioned plane. However, some lateral diffusion which is unavoidable in real cases will occur and cause the diffusion direction not to be completely perpendicular to the original joint surface. Thus, a rather ragged morphology of joint interfaces is produced, as shown in Figs 1 and 2. By inclining a small angle to the cross-sectioned plane of Fig. 3(b) and adding some lateral diffusion effects to it, a microstructural morphology similar to Fig. 1(b) can be obtained. Therefore, Fig. 3(b) is a schematic representation of the high-temperature state of sample ##2 as it was joined at 1150°C × 30 s.

Although the real holding time of sample ##1 was only about 4 s, Fig. 1(a) shows that the columnar $\alpha + \beta$ two-phase zone has already formed. This implies that the α-Ti phase or the columnar $\alpha + \beta$ two-phase zone could form almost simultaneously with the primary β-Ti layer. In addition, the isothermal solidification of step (1) might have happened during the heating stage due to the lower heating rate [19] at the end of the heating stage, as shown in Fig. 1 of Part I of this study [9]. Therefore, Fig. 1(a) shows a combined microstruc-

ture of Fig. 3(a) and (b), and it is the real microstructure of the joint interface for short t_w.

4.1.3. Step (3): The α_2-phase nucleation. The next step concerns the isothermal transformation of $\alpha \rightarrow \alpha_2$ phase, as shown in Fig. 3(c). Now, let us consider an imaginary plane parallel to the original joint surface having an Al content of about 30 at.%. This plane, called "the P plane",† is the most suitable place for the α_2 phase nucleation, as evaluated from the Ti–Al binary phase diagram and the acquired diffusion-path diagrams. Due to the successive inward diffusion of Al atoms, the P plane will gradually move away from the base metal interface. When the moving P plane passes through the already formed columnar $\alpha + \beta$ region, the original columnar α-Ti phase would transform to an α_2 phase due to the similarity in composition and hexagonal-base structure between α and α_2 phases.

As will be discussed in Section 4.2, the driving force of the $\alpha \rightarrow \alpha_2$ transformation is small at $T_w = 1150°C$, thus it needs time to push out the dissolved excess Ni(Cu) atoms from the α-phase to form an ordered α_2 structure. The lower the joining temperature, the higher the driving force and thus the shorter the needed nucleation time is. This time-dependent isothermal nucleation, called the delayed nucleation [12], will keep the α_2-layer from forming on the P plane when the time is short. In other words, the nucleation and growth of the α_2-phase on the P plane not only need proper Al contents but also require sufficient incubation time. Therefore, if the P plane moves slowly, such as when T_w is lower; or if t_w is longer enough to provide a sufficient incubation time, the α_2-phase can form at the P plane. The former case involves the temperature effects that will be discussed in Section 4.2, and the latter one to be in Section 4.1.5. In step (3) at $T_w = 1150°C$, we suggest that the P plane still moves with a rather high velocity because the Al inward diffusion rate is fast. This is due to the large Al compositional gradient that exists. Therefore, the α_2-phase nucleated along the moving P plane can not easily grow to integrate into a continuous layer due to the lack of incubation time, as shown in Fig. 3(c).

During the process in which columnar α-Ti isothermally transform to α_2, the β-Ti of $\alpha + \beta$ region located between the P plane and the base metal must also simultaneously change its phase. From the Ti–Al–Ni ternary 1150°C isotherm [16] and the acquired 1150°C diffusion-path diagrams (Fig. 4), the maximum Al content of the stable β-Ti phase is about 25at.% Al. However, these β-Ti regions located between the P plane and the base-metal have the Al% $\geqslant$ 30at.%. This feature will make these high Al-content β regions become unstable and transform to other stable phases, as shown in Fig. 3(c). They will be further discussed in the next section.

4.1.4. Step (4): The high Al% α-phase formation. Once the P plane continuously moves further away from the base–metal interface, the Al content of the layer between P plane and the base–metal interface should be higher than 30%. Under this circumstance, the α-phase will form again in this layer due to the high Al content, as seen from Figs 4 and 5. This new α-phase, called the "high Al% α-phase" in Fig. 3(d), is distinguishable from the former α-Ti phase of Fig. 3(b). This high Al% α-phase can dissolve more Ni(Cu) atoms than the ordered α_2-phase, thus it can gradually replace the isothermally-produced α_2-phase near the base metal side to form a continuous zone. The α_2-phase becomes more unstable when it is closer to the high Al% α-phase zone due to the higher Al content and the lateral diffusion of Ni(Cu) atoms. Therefore, the isothermally columnar α_2-phase nearest the high Al% α-phase side will gradually vanish, as shown in Fig. 3(d).

It is believed that the transformed β-areas have the same transformation sequence as in step (2). First, they will be separated into several smaller high Al% α and β regions by their high Al and Ni(Cu) contents and lateral diffusion. As the Al atoms continuously diffuse into these β-Ti regions, the high Al% α-phase regions become wider and wider and then they are integrated together, as shown in Fig. 3(d). Comparing Fig. 3(d) with Fig. 2(c), we can see that both of them are consistent. Therefore, Fig. 3(d) is the high-temperature state of the sample joined at 1150°C with t_w being about 42 s.

4.1.5. Step (5): The α_2-phase integration. For a long holding time, the α_2-phase will gradually grown and integrate into a continuous layer, as shown in Fig. 3(e). This feature is produced by the following phenomena in the case of a long t_w specimen. For the long holding time t_w, the Al content in liquid filler metal will gradually increase, and the Al compositional gradient between the base metal and liquid phase will successively decrease. This means that the forward diffusion rate of Al atoms decreases and the atomic lateral diffusion becomes more important. At the same time, the P plane moves with a slower velocity and the α_2-phase has enough incubation time to nucleate and grow. Finally, the α_2-phase integrates into a continuous layer.

When the α_2-phase grows and moves inward, the Ni(Cu) atoms will be more and more segregated in the residual liquid phase because their outward diffusion needs a larger and larger driving force, as

†Strictly speaking, from the micro-viewpoint, the imaginary P plane should not form a straight line parallel to the base metal interface when it passed through the $\alpha + \beta$ two-phase zone. This is because the concentrations of Al in α and β are different to begin with and the Al diffusion rates in α and β would be different due to their structural difference.

seen from the diffusion-path diagram of Fig. 4. Once the continuous α_2-layer is fully formed, this layer becomes a diffusion barrier for Ni(Cu) atoms. At this time, the outward interdiffusion rate of Ni(Cu) atoms will be further decreased if the holding time is prolonged. During the formation of α_2-phase layer, a large region of the high Al% α-phase will simultaneously appear, as mentioned in Section 4.1.4, and the interface between them will gradually become a planar one. At the same time, a β-Ti zone will be formed due to the lateral diffusion of Ni(Cu) atoms in the region nearby the filler-metal side of the original $\alpha + \beta$ zone, as shown in Fig. 3(e) in the case of the long t_w specimen. Clearly, Fig. 3(e) is in good agreement with the observed microstructure of Fig. 1(d) joined at 1150°C × 60 s. It must be pointed out that Fig. 3 aims to explain the samples joined at $T_w = 1150$°C only. For different T_w, the mechanism of Fig. 3 must be appropriately modified, as will be discussed in Section 4.2.

4.2. The effects of joining temperature T_w on the microstructural evolution

In Part I of this study [9], it has been shown that the joining temperature T_w significantly influences the microstructures of the joint interfaces. For different T_w, the corresponding ternary isotherm and stable phases are different, therefore, small variation of T_w can result in significant changes of the microstructural morphologies. From the Ti–Al binary phase diagram of Fig. 5, there is a "high Al% α-phase" $\rightarrow \alpha_2$-Ti_3Al + γ-TiAl eutectoid reaction at 1125°C, and the congruent temperature of the α_2-phase is about 1200°C. Obviously, both α_2- and high Al% α-phases are stable on the 1150°C isotherm. However, the high Al% α-phase is absent on the 1100°C isotherm and the α_2-phase is unstable on or above the 1200°C isotherm. This feature elucidates the reason why the observed microstructures of samples joined at 1100, 1150 and 1200°C show distinct interfacial morphologies.

In this study, different T_w temperatures play the major role in the microstructural evolution of Zones IV (high Al% α-phase) and V (α_2-layer) which can be explained by the degree of α_2-phase supercooling ΔT. ΔT is defined as the temperature difference between the joining temperature T_w and the congruent temperature of the α_2 phase, as shown in Fig. 5. ΔT is related to the driving force for the α-Ti $\rightarrow \alpha_2$ isothermal phase transformation at T_w.† Because the congruent temperature of the α_2-phase is about 1200°C, thus ΔT's for all joining conditions in this study are quite small. This leads to the small driving force of $\alpha \rightarrow \alpha_2$ transformation

†The true driving force is $\Delta G = (\Delta H/T_w)\Delta T$, if not considering interfacial energy. Here, the ΔH is the enthalpy of $\alpha \rightarrow \alpha_2$ transformation at T_w.

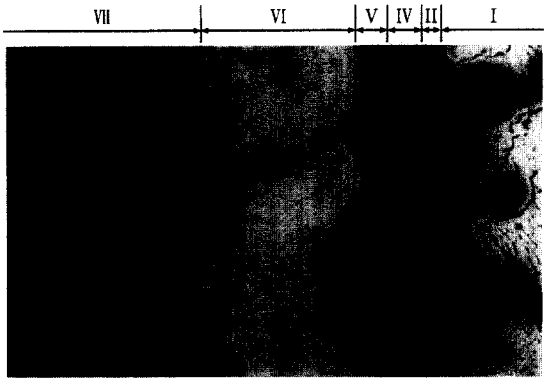

Fig. 6. The SEM interfacial microstructure of specimen joined at 1100°C × 30 s. I ~ VII express the seven characteristic interfacial zones as discussed in the text.

and the α_2-phase needs some incubation time to nucleate and grow, as mentioned in Section 4.1.3. The larger the supercooling of ΔT, the greater the driving force and the shorter the needed incubation time will be for the α_2 phase to nucleate from the α-phase, thus, the faster the continuous α_2-layer can be formed in the joint interface. For example, the sample joined at 1100°C for 30 s having ΔT = 100°C shows a continuous α_2 layer in its joint interface, as shown in Fig. 6. While samples joined at 1150°C having ΔT = 50°C show Zone III (no α_2-layer forms) with holding 30 s and Zone V

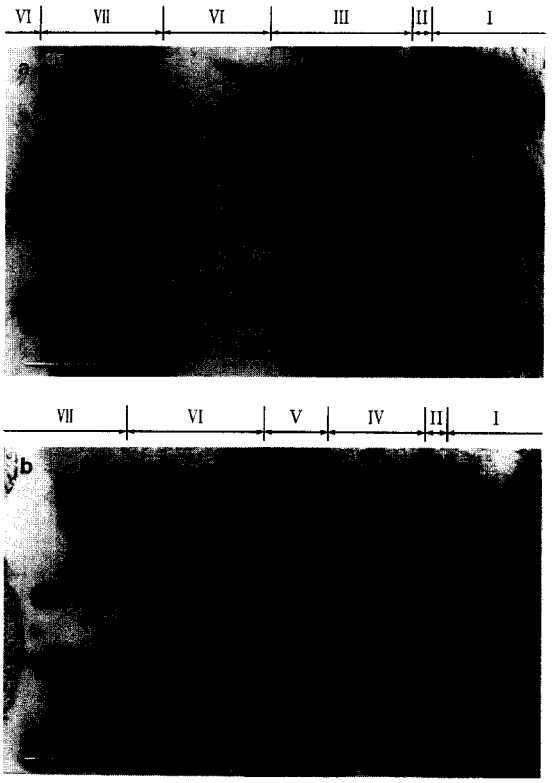

Fig. 7. The SEM interfacial microstructures of specimens joined at $T_w = 1150$°C with (a) $t_w = 30$ s (sample ##2) and (b) $t_w = 60$ s (sample ##4).

(discontinuous α_2-layer) with holding 60 s, as shown in Fig. 7(a) and (b), respectively. The sample joined at 1200°C for 30 s having $\Delta T = 0$ shows a wide Zone III without an α_2-layer being observed, as shown in Fig. 8.

Concerning the effects of different T_w on Zone IV, we must consider whether or not the high Al% α-phase exists between α_2-Ti_3Al and γ-TiAl phases on the T_w isotherm. As mentioned above, from Fig. 5 of the binary Ti–Al phase diagram, the high Al% α-phase exists on the 1150 and 1200°C isotherms, but it is absent on the 1100°C one. In addition, the disordered α-phase can dissolve more Ni(Cu) atoms than the ordered α_2 structure, this solubility characteristic also has a great effect on the room temperature microstructures of Zone IV. For example Zone IV of the specimen joined at 1150°C for 60 s [Fig. 7(b)] is formed because a high Al% α-phase exists at T_w, and has a medium ΔT and a long t_w. Specimens joined at 1100°C (Fig. 6) can form an α_2-layer more easily than specimens joined at 1150°C (Fig. 7) due to its larger ΔT. However, it is difficult for Zone IV to become a homogenized single-phase region before cooling due to the absence of high Al% α-phase at $t_w = 1100$°C. Therefore, Zone IV of the sample joined at 1100°C for 30 s is composed of black α_2 columns transformed from the original columnar α-Ti and several discontinuous precipitates transformed from the residual parts of the original β-Ti areas in $\alpha + \beta$ region. These residual precipitates, called the X-phase as mentioned in Part I of this study [9], do not readily vanish because the α_2 columns will have only small solubility of Ni(Cu) atoms. Thus, Zone IV of Fig. 6 reveals rather rare and coarse discontinuous precipitates after cooling. Although the specimen joined at 1200°C has a high Al% α-phase at T_w, its near-zero ΔT makes the formation of the α_2-layer more difficult at the joint interface. Therefore, the observed microstructure of the sample joined at 1200°C for 30 s shows a wide columnar two-phase structure of Zone III, instead of Zone IV, as shown in Fig. 8.

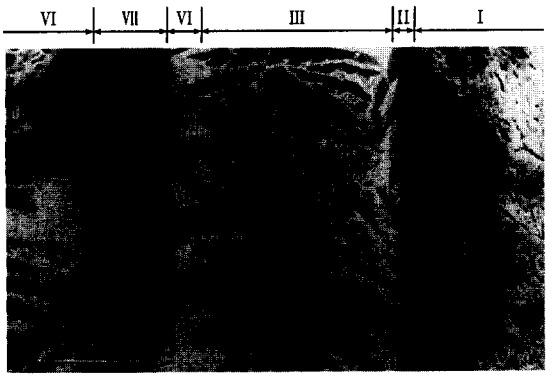

Fig. 8. The SEM interfacial microstructure of specimen joined at 1200°C × 30 s.

Certainly, some well-known kinetic effects of T_w will still act on microstructural evolution, such as the relative diffusivities of elements. The higher the joining temperature, the faster the atomic interdiffusion rate and the higher the moving P plane velocity will be. Therefore, for specimens joined at the higher T_w with a similar t_w, the entire reacting solid-state layer is thicker and formation of the α_2-layer is more difficult. This diffusivity effect can clearly be seen from the observed microstructures of Figs 6, 7(a) and 8, but this effect seems relatively less important in this study.

As mentioned above, the different T_w mainly affects the kinds of stable phases and the stability of the individual phase in each joining condition. Compared with the proposed 1150°C microstructural evolution mechanism of Fig. 3, the 1100°C one lacks step (4) due to the absence of the high Al% α-phase. Thus, its evolved microstructure shows a continuous α_2-layer and the columnar $\alpha_2 + X$ two-phase mixed morphology. On the other hand, the 1200°C one lacks step (3) and step (5) because the α_2-phase is unstable, thus its joint interface shows a wide columnar $\alpha + \beta$ two-phase structure.

5. CONCLUSIONS

The microstructural evolution of TiAl joint interfaces using Ti–15Cu–15Ni foil as brazing filler metal were investigated during infrared joining at 1150°C under different holding times. Because of the sensitive responses of infrared joining, the microstructural evolution of joint interfaces can be effectively realized. In order to clarify how or why the observed multilayered structures formed, a five-step microstructural evolution mechanism at 1150°C joining temperature is proposed in this study. These time-dependent evolution steps, which are based on the observed microstructures, include (a) β-Ti layer formation, (b) columnar $\alpha + \beta$ two-phase zone formation, (c) α_2-phase nucleation, (d) high Al% α-phase formation and (e) α_2-phase integration. These steps are consistent with the multiphase diffusion theories in solid-state systems. These features support the primary viewpoint of this study that the acquired multilayered structures have formed before cooling due to isothermal solidification and thereafter solid-state interdiffusion. The different joining temperature (T_w) effects are also investigated in this study. According to the proposed evolution mechanism, the different T_w mainly affects the kinds of stable phases and the stability of individual phases in each joining condition. Because different joining temperatures, T_w, have different corresponding ternary isotherms and stable phases, small variation of T_w can result in significant changes of the microstructural morphologies. The microstructural evolution of zones of α_2- and high Al% α-phases can be explained by

the degree of α_2-phase supercooling ΔT. The lower the joining temperature, the more the supercooling of ΔT. The higher the driving force of the ordered α_2 nucleated from the α-Ti, the faster the continuous α_2-layer can be formed in the joint interface. The proposed microstructural evolution mechanism of this study can clearly elucidate the observed interfacial microstructures at ambient temperatures.

Acknowledgements—The authors sincerely acknowledge the financial support of this research by the National Science Council (NSC), Republic of China, by the Grant NSC82-0405-E002-402.

REFERENCES

1. Patterson, R. A., Martin, P. L., Damkroger, B. K. and Christodoulou, L., *Welding Journal*, 1990, **69**, 39s.
2. Baeslack, I. I. I. W. A., Mascorella, T. J. and Kelly, T. J., *Welding J.*, 1989, **68**, 483s.
3. Mallory, L. C., Baeslack, I. I. I. W. A. and Phillips, D., *J. Mater. Sci. Lett.*, 1994, **13**, 1061.
4. Nakao, Y., Shinozaki, K. and Hamada, M., *ISIJ Int.*, 1991, **31**, 1260.
5. Yan, P. and Wallach, E. R., *Intermetallics*, 1993, **1**, 83.
6. Cam, G., Bohm, K.-H., Mullauer, J. and Kocak, M., *J.O.M.*, 1996, **48**, 68.
7. Annaji, S., Lin, R. Y. and Wu, S. K., in *Proc. Design Fundamentals High Temperature Composites, Intermetallics and Metal–Ceramics Systems*, ed. R. Y. Lin, Y. A. Chang, R. G. Reddy and C. T. Lui. TMS, Warrendale, PA, 1995, p. 125.
8. Blue, C. A., Blue, R. A. and Lin, R. Y., *Scripta metall. mater.*, 1995, **32**, 127..
9. Lee, S. J., Wu, S. K. and Lin, R. Y., *Acta mater.* 1998, **46,** 1283.
10. Reed-Hill, R. E., *Physical Metallurgy Principles* 2nd edn. Van Nostrand, Princeton, NJ. 1973, p. 559.
11. van Loo, F. J. J., *Prog. Solid. St. Chem.*, 1990, **20**, 47.
12. Kirkaldy, J. S., *Diffusion in the Condensed State* Institute of Metals, London. 1987, p. 361.
13. Kim, Y.-W. and Dimiduk, D. M., *J.O.M.*, 1991, **43**, 40.
14. McCullough, C., Valencia, J. J., Levi, C. G. and Mehrabian, R., *Acta metall. mater.*, 1989, **37**, 1321.
15. Murray, J. L., in *Binary Alloy Phase Diagrams*, ed. T. B. Massalski, J. L. Murray, L. H. Bennelt and H. Baker. ASM, Metal Park, OH, 1986, p. 1763.
16. Lee, K. J. and Nash, P., *J. of Phase Equilibria*, 1991, **12**, 551.
17. Collings, E. W., *The Physical Metallurgy of Titanium Alloys* ASM, Metal Park, OH. 1984, p. 390.
18. Gegel, H. L., in *The Physical Metallurgy of Titanium Alloys*, ed. E. W. Collings. ASM, Metal Park OH, 1984, p. 65.
19. Zhou, Y., Gale, W. F. and North, T. H., *Int. Mater. Rev.*, 1995, **40**, 181.